Available online at www.sciencedirect.com
SCIENCE DIRECT®
Coordination Chemistry Reviews 245 (2003) 107–120
COORDINATION CHEMISTRY REVIEWS
www.elsevier.com/locate/ccr

Vibrational spectroscopic properties of molybdenum and tungsten N_2 and N_2H_x complexes with depe coligands: comparison to dppe systems and influence of H-bridges

Felix Tuczek*, Kay H. Horn, Nicolai Lehnert

Institut für Anorganische Chemie, Christian Albrechts Universität, Olshausenstrasse 40, D-24098 Kiel, Germany

Received 5 December 2002; accepted 14 April 2003

Contents

Abstract ... 107
1. Introduction ... 107
2. Experimental and computational procedures ... 108
2.1. Sample preparation, isotopic substitution ... 108
2.2. IR spectroscopy ... 108
2.3. Raman spectroscopy ... 109
2.4. DFT calculations ... 109
2.5. Normal coordinate analysis ... 109
3. Structural parameters and models ... 110
4. Vibrational spectroscopy and QCA-NCA ... 110
4.1. Dinitrogen complexes $\mathbf{1}^{Mo}_{depe}$ and $\mathbf{1}^{W}_{depe}$ ... 110
4.2. Mo–N_2H_2 complex $\mathbf{3}^{Mo}_{depe}$ ... 115
5. Discussion ... 118
Acknowledgements ... 119
References ... 119

Abstract

The vibrational structures of the dinitrogen complexes $[M(N_2)_2(depe)_2]$, M = Mo, W, and the NNH_2 complex $[MoCl(NNH_2)(depe)_2]Cl$ derived from $[Mo(N_2)_2(depe)_2]$ by protonation with HCl are investigated with the help of infrared and Raman spectroscopy (depe = 1,2-bis(diethylphosphino)ethane). Vibrational data obtained from natural abundance-N, ^{15}N and ^{2}H isotope substituted derivatives are evaluated with the quantum-chemistry assisted normal coordinate analysis procedure, giving an experimentally calibrated force field for these systems. The results of this treatment are compared with those obtained on analogous dppe complexes (dppe = 1,2-bis(diphenylphosphino)ethane). The N–N frequencies and force constants of the dinitrogen complexes $[M(N_2)_2(diphos)_2]$, M = Mo and W, diphos = depe, dppe, indicate an activation of N_2 in the order $[W(N_2)_2(depe)_2]>[W(N_2)_2(dppe)_2]\approx[Mo(N_2)_2(depe)_2]>[Mo(N_2)_2(dppe)_2]$. The spectra of $[MoCl(NNH_2)(depe)_2]Cl$ show significant differences with respect to those of $[WF(NNH_2)(dppe)_2]BF_4$ which are ascribed to a dimeric structure of the Mo–depe complex, being bridged by two Cl^- anions. The results obtained on the dinitrogen complexes are considered within a broader range of Mo– and W–NNH_x systems with dppe and depe coligands, and the evolution of force constants upon successive protonation of the N_2 ligand are discussed.

Keywords: IR spectroscopy; Raman spectroscopy; Vibrational spectroscopy

1. Introduction

The reduction and protonation of dinitrogen at ambient conditions is one of the great challenges of chemistry [1]. In nature this process is mediated by the enzyme

* Corresponding author. Tel.: +49-431-880-2406; fax: +49-431-880-1520.
E-mail address: ftuczek@ac.uni-kiel.de (F. Tuczek).

0010-8545/$ – see front matter © 2003 Elsevier B.V. All rights reserved.
doi:10.1016/S0010-8545(03)00064-X

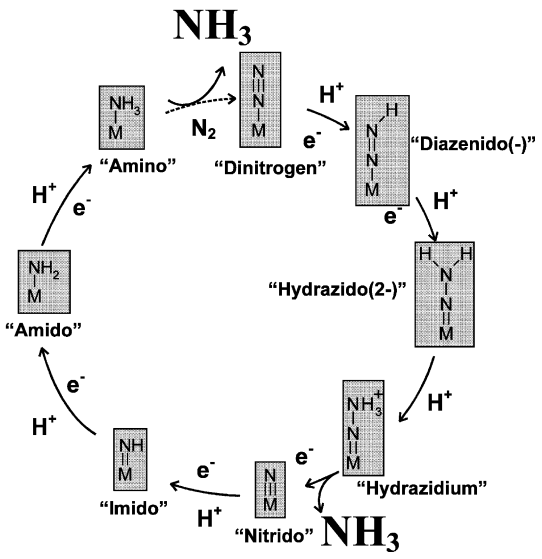

Scheme 1.

nitrogenase which binds and reduces the N_2 molecule at a unique Fe/Mo/S cluster, the iron-molybdenum cofactor (FeMoco) [2]. Although the crystal structure of nitrogenase was determined about 10 years ago and new information has been obtained recently [3], no detailed insight at the molecular level into the mechanism of N_2 reduction by this enzyme exists yet. Nevertheless, it is possible to bind and reduce dinitrogen at simple mono- and bi-nuclear transition-metal systems allowing to obtain mechanistic information on the elemental steps involved in this process. If 'moderately' activating systems containing Mo and W phosphine complexes are employed [4], all the intermediates along the following reduction pathway can be isolated [5] (Scheme 1).

This end-on terminal reduction mode of N_2 has been suggested to apply to nitrogenase as it is compatible with the Thorneley/Lowe kinetic scheme [6]. In previous work, we studied the N_2, N_2H, and N_2H_2 complexes $[W(N_2)_2(dppe)_2]$ ($\mathbf{1}^{W}_{dppe}$; dppe = 1,2-bis(diphenylphosphino)ethane, $[WF(NNH)(dppe)_2]$ ($\mathbf{2}^{W}_{dppe}$) and $[WF(NNH_2)(dppe)_2]^+$ ($\mathbf{3}^{W}_{dppe}$) with the help of infrared and Raman spectroscopy coupled to DFT calculations and found that the stepwise protonation is accompanied by a successive reduction of N–N bond order and a concomitant increase in metal–ligand covalency [7].

More recently, these studies were complemented by the investigation of Mo and W hydrazidium complexes $[MF(NNH_3)(depe)_2](BF_4)_2$, M = Mo ($\mathbf{4}^{Mo}_{depe}$) and W ($\mathbf{4}^{W}_{depe}$; depe = 1,2-bis(diethylphosphino)ethane) [8]. Analogous NNH_3 compounds with dppe coligands do not exist since protonation of the corresponding N_2 precursors gives NNH_2 complexes [9]. The hydrazidium complexes $\mathbf{4}^{Mo}_{depe}$ and $\mathbf{4}^{W}_{depe}$ are prepared from the N_2 complexes $[M(N_2)_2(depe)_2]$, M = Mo ($\mathbf{1}^{Mo}_{depe}$) and W ($\mathbf{1}^{W}_{depe}$), by protonation with HBF_4 [10]. We found that treatment of $\mathbf{1}^{Mo}_{depe}$ and $\mathbf{1}^{W}_{depe}$ with HCl, on the other hand, leads to the NNH_2 compounds $[MCl(NNH_2)(depe)_2]Cl$, M = Mo ($\mathbf{3}^{Mo}_{depe}$) and W ($\mathbf{3}^{W}_{depe}$) [8]. In this paper, the results of vibrational spectroscopy obtained on the Mo and W–N_2 and –NNH_2 depe complexes $\mathbf{1}^{Mo}_{depe}$, $\mathbf{1}^{W}_{depe}$ and $\mathbf{3}^{Mo}_{depe}$ are presented. As before, vibrational data are evaluated with a quantum-chemistry assisted normal coordinate analysis (QCA-NCA) [7a], giving experimentally calibrated force fields for all of the compounds investigated. These results are compared with data obtained both on the analogous dppe complexes $\mathbf{1}^{Mo}{}_{dppe}$, $\mathbf{1}^{W}_{dppe}$ and $\mathbf{3}^{W}_{dppe}$, and on the corresponding hydrazidium compounds $\mathbf{4}^{Mo}_{depe}$ and $\mathbf{4}^{W}_{depe}$. Based on the N–N force constants and frequencies of the various dinitrogen systems **1**, the relative degrees of N_2 activation by the bidentate phospine ligands depe and dppe and the two metal centers Mo and W, respectively, can be assessed. Consideration of the N–N and metal–N force constants of the protonated derivatives $[MX(NNH_x)(diphos)_2]^{(x-1)+}$, M = Mo, W; X = Cl, F; diphos = dppe, depe; $x = 1$ (**2**), 2 (**3**) and 3 (**4**), on the other hand, allows one to monitor the evolution of the N–N triple bond to a single bond as well as the increase of metal–ligand covalency upon successive protonation. This provides valuable insight into details of the reduction and protonation of N_2 as well as the dependence of this process upon the choice of the metal and the ligand system.

2. Experimental and computational procedures

2.1. Sample preparation, isotopic substitution

The natural abundance isotope dinitrogen complexes $[Mo(N_2)_2(depe)_2]$ (^{14}N-$\mathbf{1}^{Mo}_{depe}$) and $[W(N_2)_2(depe)_2]$ (^{14}N-$\mathbf{1}^{W}_{depe}$) were prepared following literature procedures [11]. For the synthesis of the corresponding NNH_2 species $[MoCl(NNH_2)(depe)_2]Cl$ (^{14}N-$\mathbf{3}^{Mo}_{depe}$) and $[WCl(NNH_2)(depe)_2]Cl$ (^{14}N-$\mathbf{3}^{W}_{depe}$), anhydrous HCl was condensed onto the dinitrogen complexes ^{14}N-$\mathbf{1}^{Mo}_{depe}$ and ^{14}N-$\mathbf{1}^{W}_{depe}$, respectively, at −196 °C, similar to a procedure described by Galindo [12]. The ^{15}N isotopomers $[Mo(^{15}N_2)_2(depe)_2]$ (^{15}N-$\mathbf{1}^{Mo}_{depe}$) and $[W(^{15}N_2)_2(depe)_2]$ (^{15}N-$\mathbf{1}^{W}_{depe}$) were synthesised using $^{15}N_2$. The preparation of the protonated, ^{15}N labeled, complex $[MoCl(^{15}N^{15}NH_2)(depe)_2]Cl$ (^{15}N-$\mathbf{3}^{Mo}_{depe}$) was carried out from the ^{15}N substituted dinitrogen complex ^{15}N-$\mathbf{1}^{Mo}_{depe}$. The reactions and sample preparations were performed under a nitrogen or argon atmosphere using Schlenk-techniques. Sample manipulations for vibrational and optical spectroscopy were carried out in a glovebox. All solvents were dried under argon.

2.2. IR spectroscopy

Middle-infrared (MIR) spectra were obtained on KBr pellets using a Mattson Genesis Type I Spectrometer. Far-infrared (FIR) spectra were obtained on RbI pellets using a Bruker IFS 66s FTIR spectrometer. Both instruments

are equipped with a Cryogenic (CTI) helium cryostat. The spectra were recorded at 10 K and the resolution was set to 2 cm^{-1}.

2.3. Raman spectroscopy

Raman spectra were obtained on a Bruker IFS 66/CS NIR FT-Raman spectrometer at 270 K. The setup involves a 350 mW NdYAG-Laser with an excitation wavelength of 1064 nm. The samples were pressed into the groove of a holder which can be sealed with a glass plate to ensure inert gas conditions

2.4. DFT calculations

Input parameters and results of the calculations are given in Ref. [7b]. Spin-restricted DFT calculations were carried out for the model systems $[Mo(N_2)_2(PH_3)_4]$ ($\tilde{\mathbf{1}}$) and $[MoF(NNH_2)(PH_3)_4]^+$ ($\tilde{\mathbf{3}}$) of $\mathbf{1}^{Mo}_{depe}$, $\mathbf{1}^{W}_{depe}$ and $\mathbf{3}^{Mo}_{depe}$, respectively, using Becke's three parameter hybrid functional with the correlation functional of Lee, Yang and Parr (B3LYP) [13] The LANL2DZ basis set was used. It applies Dunning/Huzinaga full double zeta (D95) [14] basis functions on first row and Los Alamos effective core potentials plus DZ functions on all other atoms [15]. The f matrix in internal coordinates was extracted from the Gaussian output using the program Redong [16].

2.5. Normal coordinate analysis

Normal coordinate calculations were performed using the QCPE computer program 576 by M.R. Peterson and D.F. McIntosh. It involves solution of the secular equation $GFL = \lambda L$ by the diagonalization procedure of Miyazawa [17]. The calculations are based on a general valence force field, and the force constants are refined using the nonlinear optimization routine of the simplex algorithm according to Nelder and Mead [18]. Normal coordinate analysis is based on the QCA-NCA procedure which involves generation of an initial force field by DFT treatment of $\tilde{\mathbf{1}}$ and $\tilde{\mathbf{3}}$, respectively (vide supra) [7a]. In order to remove artificial interactions between the PH_3 moieties of these models and the rest of the molecule, the PH_3 ligands were simplified to P atoms, leading to models $\mathbf{1}'$ and $\mathbf{3}'$, respectively. In addition, the F-ligand of $\tilde{\mathbf{3}}$ was exchanged with Cl in $\mathbf{3}'$, enlarging the metal–ligand bond distance to 2.4 Å. The corresponding f-matrices f′ can be divided into two parts: the force constants of the NN–M–NN and F–M–N–NH_2 unit, respectively, (core) and the force constants of the MP_4 unit (frame). The force constants of the frame and non-diagonal elements between the core and the frame were adapted from the DFT calculation and fixed. Very small matrix elements were neglected. The force constants of the core were fitted to match the experimental frequencies, taking the DFT values as initial guess.

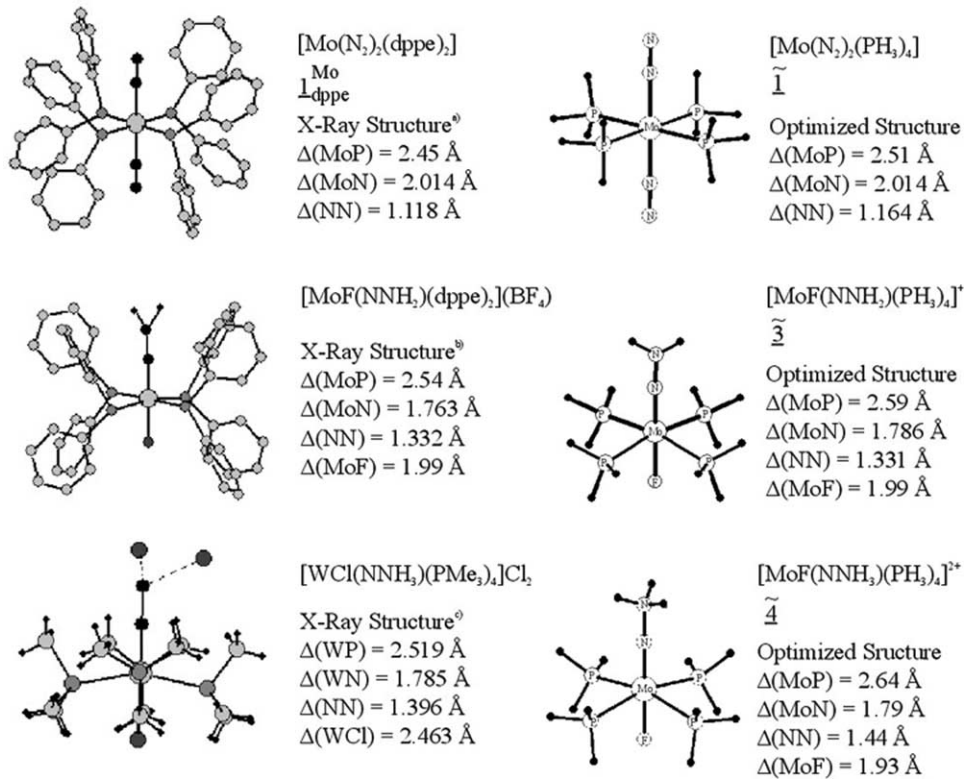

Fig. 1. Structurally characterized examples of Mo and W dinitrogen and hydrazido(2−) complexes and model systems (a) T. Uchida, Y. Uchida, M. Hidai, T. Kodama, Acta Crystallogr., B31 (1975) 1197. (b) M. Hidai, T. Kodama, M. Sato, M. Harakawa, Y. Uchida, Inorg. Chem., 15 (1976) 2694. (c) A. Galindo, A. Hills, D. L. Hughes, R. L.Richards, J. Chem. Soc. Dalton Trans. (1990), 283.

Table 1
Mo/W–N_2, –NNH, –NNH_2 and –NNH_3 complexes and corresponding models: bond lengths from X-ray and DFT geometry optimization

	Model/compound		M–P	M–N	N–N	M–X	N–H	Reference
$[Mo(N_2)_2(PH_3)_4]$	$\tilde{\mathbf{1}}$	Opt	2.510	2.014	1.164	–	–	[7b]
$[Mo(N_2)_2(dppe)_2]$	$\mathbf{1}^{Mo}_{dppe}$	X-ray	2.45	2.014	1.118	–	–	[a]
$[MoF(NNH)(PH_3)_4]$	$\tilde{\mathbf{2}}$	Opt	2.54	1.826	1.276	2.07 [b]	1.083	[7b]
$[MoF(NNH_2)(PH_3)_4]^+$	$\tilde{\mathbf{3}}$	Opt	2.594	1.786	1.331	1.99 [b]	1.01	[7b]
$[MoF(NNH_2)(dppe)_2]^+$	$\mathbf{3}^{Mo}{}_{dppe}$	X-ray	2.54	1.763	1.332	1.99 [b]	1.09	[c]
$[WCl(NNH_2)(dppe)_2]^+$	$\mathbf{3}^{W}_{dppe}$	X-ray	~2.5	1.73	1.37	2.42 [d]	–	[e]
$[WF(NNH_2)(depe)_2]^+$	$\mathbf{3}^{W}_{depe}$	X-ray	~2.5	1.771	1.355	2.027 [f]		10
$[MoF(NNH_3)(PH_3)_4]^{2+}$	$\tilde{\mathbf{4}}$	Opt	2.64	1.79	1.44	1.93 [b]	1.04	8
$[WCl(NNH_3)(PMe_3)_4]^{2+}$	$\mathbf{4}^{W}_{PMe_3}$	X-ray	2.519	1.785	1.396	2.463 [d]	–	12

[a] T. Uchida, Y. Uchida, M. Hidai, T. Kodama, Acta Crystallogr., B31 (1975) 1197.
[b] Mo–F.
[c] M. Hidai, T. Kodama, M. Sato, M. Harakawa, Y. Uchida, Inorg. Chem., 15 (1976) 2694.
[d] W–Cl.
[e] G.A. Heath, R. Mason, K.M. Thomas, J. Am. Chem. Soc., 96 (1974) 259.
[f] W–F.

3. Structural parameters and models

Vibrational analysis of the dinitrogen complexes $\mathbf{1}^{Mo}_{depe}$, $\mathbf{1}^{W}_{depe}$ and the NNH_2 complex $\mathbf{3}^{Mo}_{depe}$ is based on the QCA-NCA procedure which we have developed earlier in order to account for the vibrational properties of the analogous dppe systems $\mathbf{1}^{Mo}{}_{dppe}$, $\mathbf{1}^{W}_{dppe}$ and $\mathbf{3}^{W}_{dppe}$ [7a]. It requires the previous DFT treatment of corresponding models $\tilde{\mathbf{1}}$ and $\tilde{\mathbf{3}}$, respectively, including geometry optimization [7a]. Analogous calculations have been performed for the diazenido(−) systems $\mathbf{2}^{W}_{dppe}$ [7b] and the hydrazidium complexes $\mathbf{4}^{Mo}_{depe}$ and $\mathbf{4}^{W}_{depe}$, [8] respectively.

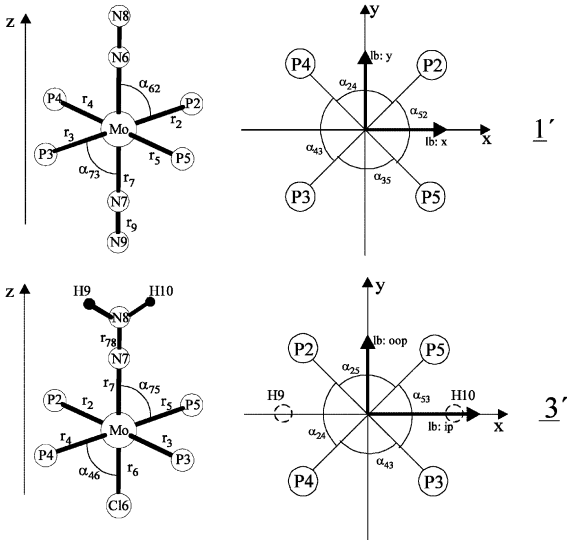

Scheme 2.

Fig. 1 shows structurally characterized examples of Mo and W dinitrogen and hydrazido-(2−) complexes as well as model systems $\tilde{\mathbf{1}}$ and $\tilde{\mathbf{3}}$ derived from these structures. A structurally characterized hydrazidium complex **4** along with the corresponding model $\tilde{\mathbf{4}}$ is given for comparison. X-ray structures of diazenido(−) complexes **2** do not exist; structural information on these systems is therefore obtained from geometry optimization of a corresponding model $\tilde{\mathbf{2}}$ [7b]. Experimentally determined bond lengths are compared with values derived from DFT geometry optimizations of models $\tilde{\mathbf{1}}$–$\tilde{\mathbf{4}}$ in Table 1. For QCA-NCA treatment of $\mathbf{1}^{Mo}_{depe}$, $\mathbf{1}^{W}_{depe}$ and $\mathbf{3}^{Mo}_{depe}$, models $\tilde{\mathbf{1}}$and $\tilde{\mathbf{3}}$ are modified to models $\mathbf{1}'$ and $\mathbf{3}'$, respectively, which are shown in Scheme 2 along with internal coordinate definitions and coordinate systems.

4. Vibrational spectroscopy and QCA-NCA

4.1. Dinitrogen complexes $\mathbf{1}^{Mo}_{depe}$ and $\mathbf{1}^{W}_{depe}$

Vibrational spectra of the $[M(N_2)_2(depe)_2]$ complexes $\mathbf{1}^{Mo}_{depe}$ and $\mathbf{1}^{W}_{depe}$ are given in Figs. 2–5. Interpretation of these spectra is based on the model system $[M(N_2)_2P_4]$ ($\mathbf{1}'$) of D_{2h} symmetry (Scheme 2). The eight normal modes of the central N–N–M–N–N unit of $\mathbf{1}'$ are the symmetric and antisymmetric stretching modes of the M–N and N–N bonds, $\nu_{s/as}$(MN) and $\nu_{s/as}$(NN), respectively, and the four linear bends $\delta_{s/as}$(MNN), two in each orthogonal direction *x* and *y*. The four symmetric modes are Raman, the antisymmetric ones IR active. Experimentally observed vibrations are collected along with isotope shifts and assignments in Table 2 for the Mo systems ^{14}N-$\mathbf{1}^{Mo}_{depe}$, ^{15}N-$\mathbf{1}^{Mo}_{depe}$ and in Table 3 for the W systems ^{14}N-$\mathbf{1}^{W}_{depe}$ and ^{15}N-$\mathbf{1}^{W}_{depe}$.

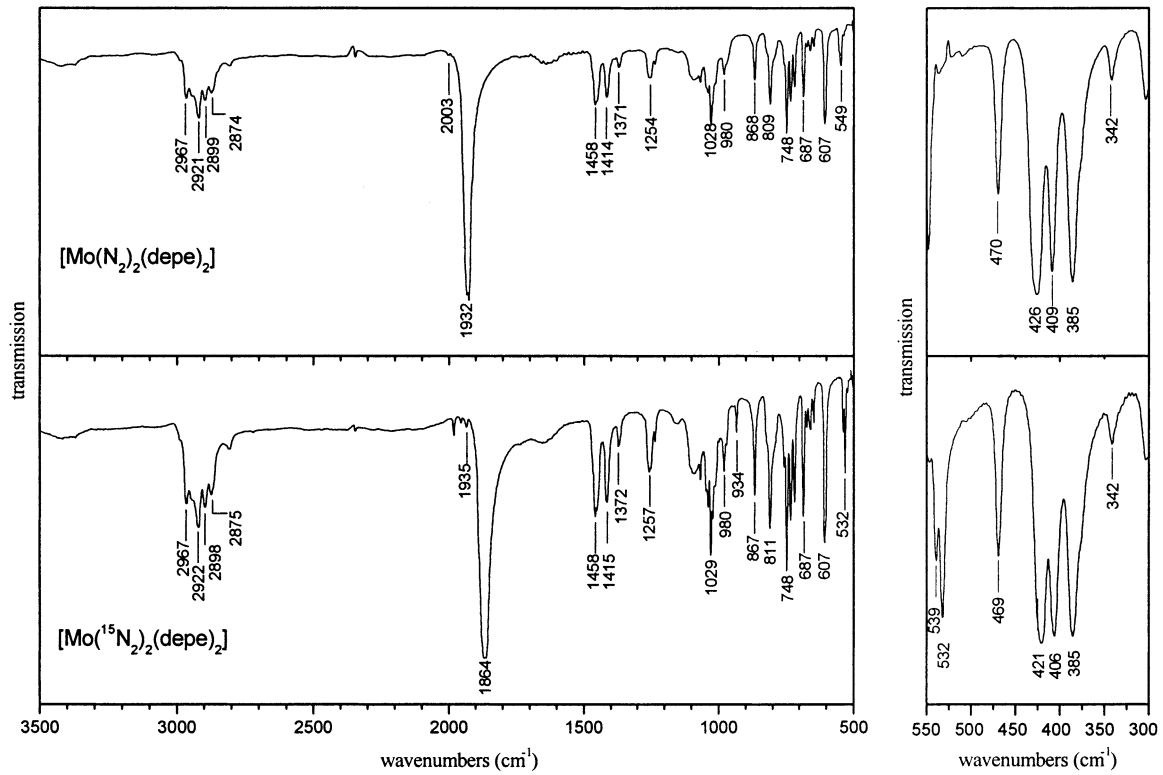

Fig. 2. IR spectra of $[Mo(N_2)_2(depe)_2]$ (^{14}N-$\mathbf{1}^{Mo}_{depe}$) and $[Mo(^{15}N_2)_2(depe)_2]$ (^{15}N-$\mathbf{1}^{Mo}_{depe}$).

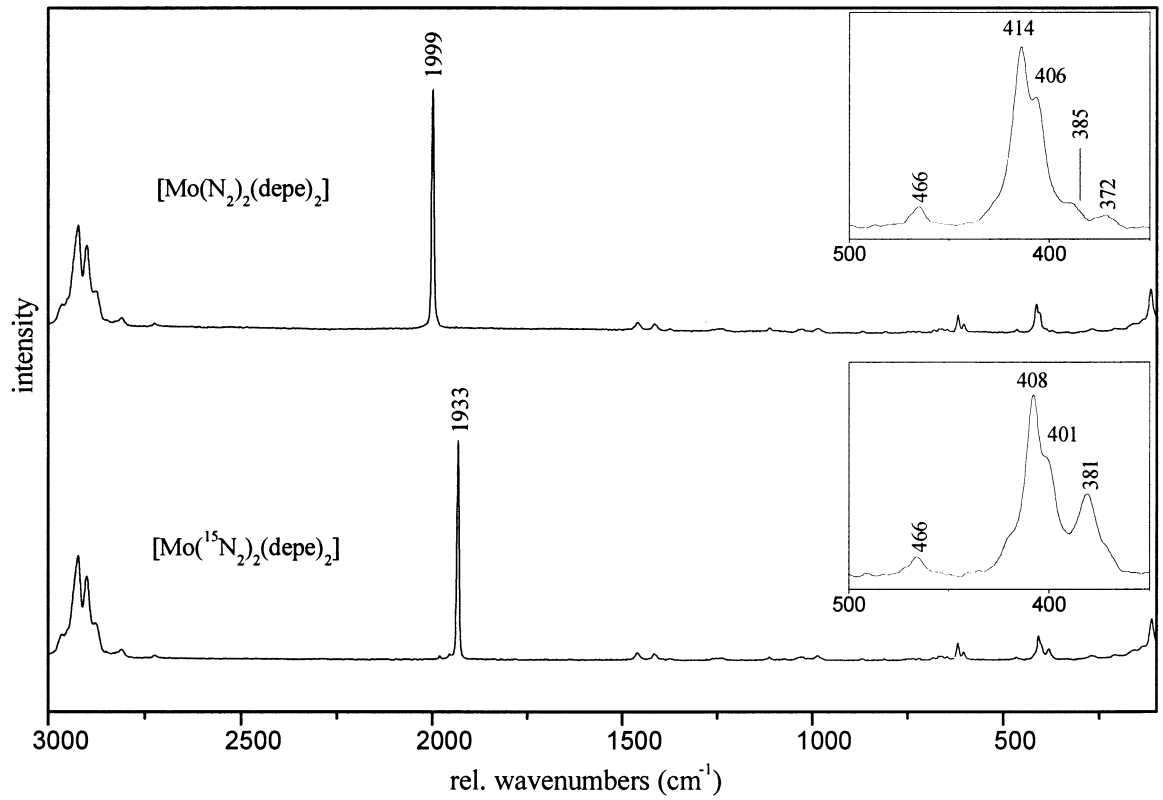

Fig. 3. Raman spectra of $[Mo(N_2)_2(depe)_2]$ (^{14}N-$\mathbf{1}^{Mo}_{depe}$) and $[Mo(^{15}N_2)_2(depe)_2]$ (^{15}N-$\mathbf{1}^{Mo}_{depe}$).

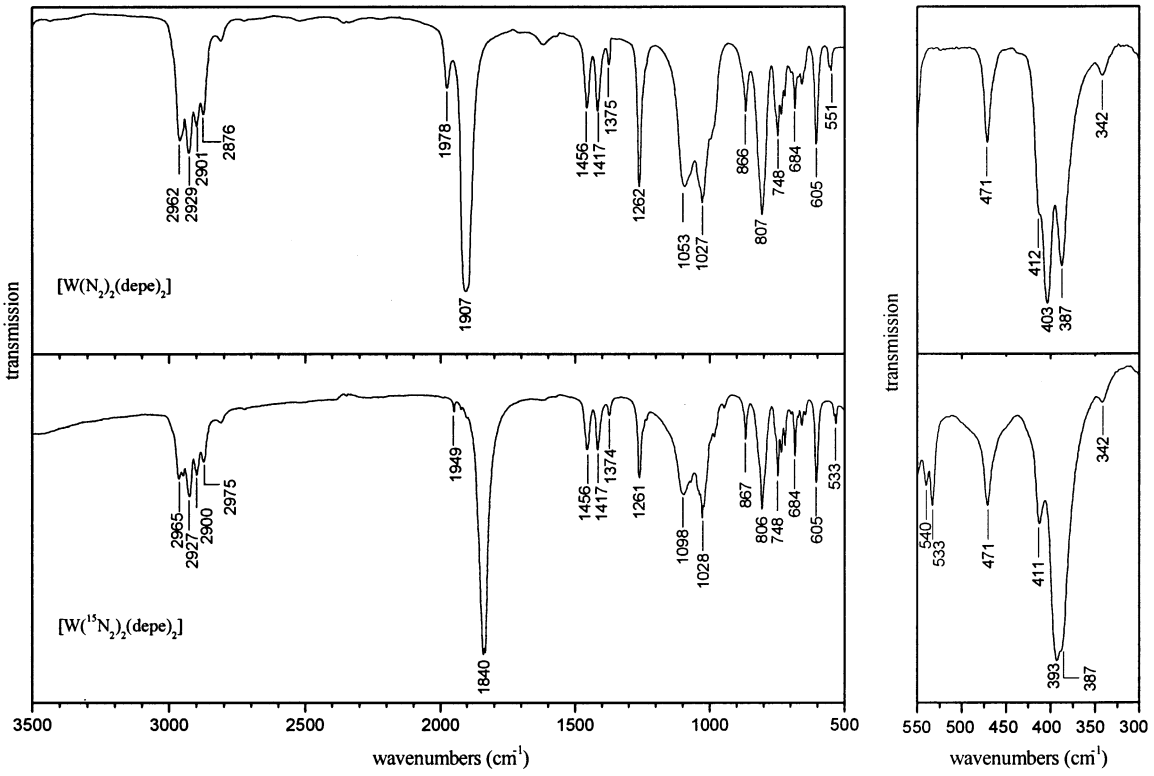

Fig. 4. IR spectra of $[W(N_2)_2(depe)_2]$ (^{14}N-$\mathbf{1}^{W}_{depe}$) and $[W(^{15}N_2)_2(depe)_2]$ (^{15}N-$\mathbf{1}^{W}_{depe}$).

IR spectra of ^{14}N-$\mathbf{1}^{Mo}_{depe}$ and ^{15}N-$\mathbf{1}^{Mo}_{depe}$ are given in Fig. 2. The IR active stretching vibration ν_{as}(NN) is assigned to the prominent peak at 1932 cm^{-1} which upon ^{15}N substitution shifts to 1864 cm^{-1}. The second isotope sensitive peak is assigned to the linear bends δ_{as}(MoNN) at 549 cm^{-1}. In the spectrum of the ^{15}N substituted compound this feature appears split into two bands at 539 and 532 cm^{-1}, corresponding to a correlation splitting or a lifting of the twofold degeneracy of this vibration (see below). The metal–N stretching vibration ν_{as}(MoN) is found at 426 cm^{-1}, shifting to 421 cm^{-1} in the ^{15}N compound. Vibrational modes of the depe ligand are located at 470 (band I), 409 (band II) and 385 cm^{-1} (band III); peaks at comparable positions also appear in Raman spectra (see below) [19]. There is apprecia-

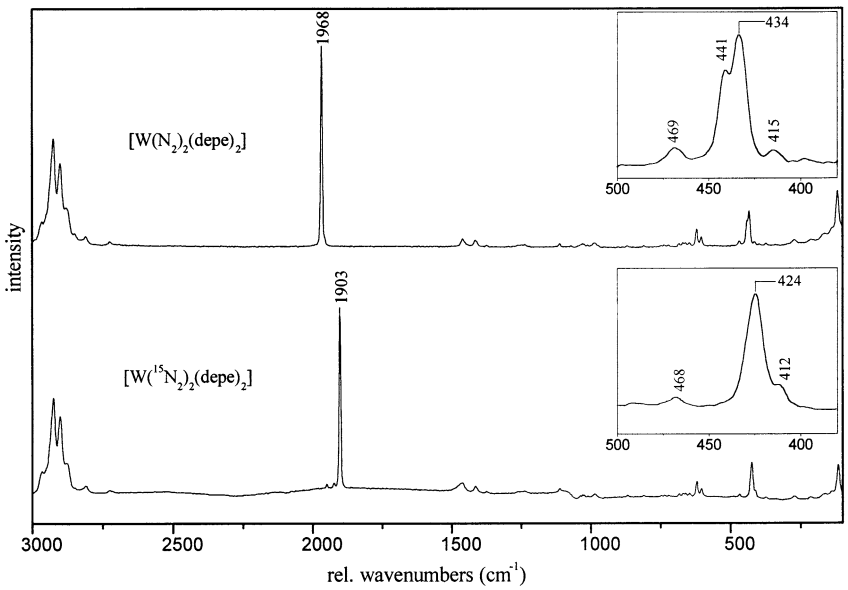

Fig. 5. Raman spectra of $[W(N_2)_2(depe)_2]$ (^{14}N-$\mathbf{1}^{W}_{depe}$) and $[W(^{15}N_2)_2(depe)_2]$ (^{15}N-$\mathbf{1}^{W}_{depe}$).

Table 2
Observed and calculated frequencies of $[Mo(N_2)_2(depe)_2]$ ($\mathbf{1}^{Mo}_{depe}$) in cm^{-1}

	Experimental		QCA-NCA		B3LYP
	N_2	$^{15}N_2$	N_2	$^{15}N_2$	
ν_s(NN)	1999	1933	2000	1932	1992
ν_{as}(NN)	1932	1864	1931	1865	1953
δ_s(MoNN)^x	n.o.	n.o.	465	450	411
δ_s(MoNN)^y					410
δ_{as}(MoNN)^x	n.o.	539	551	534	567
δ_{as}(MoNN)^y	549	532			560
I	470(IR), 466(R)	469(IR), 466(R)			
ν_{as}(MoN)	426	421	426	411	437
ν_s(MoN)	414	408	414	406	452
II	409(IR), 406(R)	406(IR), 401(R)			
III	385(IR), 385(R)	385(IR), 381(R)			

ble mixing between ν_{as}(MoN) and the depe vibration II, as evident from the isotope shift of the latter band from 409 to 406 cm^{-1}.

The Raman spectra of ^{14}N-$\mathbf{1}^{Mo}_{depe}$ and ^{15}N-$\mathbf{1}^{Mo}_{depe}$ given in Fig. 3 shows strong resonance enhancement of the vibrations of the NN–Mo–NN unit. The symmetric stretching mode ν_s(NN) is found at 1999 and shifts to 1933 cm^{-1} upon ^{15}N substitution. The ν_s(MoN) mode shifts from 414 to 408 cm^{-1} where strong mixing with band II occurs. This is evident from a 3 to 5 cm^{-1} isotope shift of the latter feature (Table 2). The 381 cm^{-1} peak in the ^{15}N spectrum corresponds to band III which by admixture of ν_s(MoN) gains intensity and is shifted from its original position at ∼385 cm^{-1}. In agreement with previous experience [7a,19], and the literature [20], linear bends ($\delta_s{}^{x,y}$) are weak or not observed in the Raman spectra.

Fig. 4 gives the IR spectra of ^{14}N-$\mathbf{1}^{W}_{depe}$ and ^{15}N-$\mathbf{1}^{W}_{depe}$. By analogy to the Mo spectrum, the features at 471, 412 and 387 cm^{-1} are identified as bands I, II and III of the depe ligand. The N–N stretching vibration ν_{as}(NN) (IR active) at 1907 cm^{-1} shifts on ^{15}N substitution to 1840 cm^{-1}. Two other isotope sensitive peaks are found in the spectra: The two peaks at 557 and 551 which shift to 540 and 533 in the ^{15}N compound, respectively, are assigned to the linear bends δ_{as}(WNN) in *x* and *y* direction. In contrast, the analogous dppe compound shows no splitting for this vibration [7a]. The band at 403 cm^{-1}, shifting to 393 cm^{-1} upon ^{15}N substitution is identified as the antisymmetric W–N stretch, ν_{as}(WN).

In the Raman spectrum of ^{14}N-$\mathbf{1}^{W}_{depe}$ (Fig. 5), ν_s(NN) belongs to the intense peak at 1968 cm^{-1} which shifts to 1903 cm^{-1}. The Raman-forbidden mode ν_{as}(NN) is not observed. The symmetric W–N stretching vibration must be associated with the features at 441 and 434. As the spectrum of the corresponding ^{15}N substituted complex exhibits only one peak at 424 cm^{-1}, we conclude that the 441 cm^{-1} peak in the ^{14}N spectrum is only enhanced by mixing with ν_s(WN) which is identified with the peak at 434 cm^{-1}. The peak at 415 cm^{-1} peak which has shifted to 412 cm^{-1} is assigned to band II. As usual, the linear bending vibrations are of low intensity in the Raman experiment and are not observed in the spectrum (vide supra).

Normal coordinate analysis of the vibrational data of $\mathbf{1}^{Mo}_{depe}$ and $\mathbf{1}^{W}_{depe}$ is performed by the QCA-NCA procedure, based on model $\mathbf{1}'$. Details of this QCA-NCA treatment, in-

Table 3
Observed and calculated frequencies of $[W(N_2)_2(depe)_2]$ ($\mathbf{1}^{W}_{depe}$) in cm^{-1}

	Experimental		QCA-NCA		B3LYP [a]
	N_2	$^{15}N_2$	N_2	$^{15}N_2$	
ν_s(NN)	1968	1903	1969	1902	1992
ν_{as}(NN)	1907	1840	1906	1841	1953
δ_s(WNN)^x	n.o.	n.o.	462	446	411
δ_s(WNN)^y					410
δ_{as}(WNN)^x	557	540	554	536	567
δ_{as}(WNN)^y	551	533			560
I	471(IR), 469(R)	471(IR), 468(R)			
ν_s(WN)	434	424	435	424	452
II	412(IR), 415(R)	411(IR), 412(R)			
ν_{as}(WN)	403	393	405	391	437
III	387(IR)	387(IR)			

[a] Calculated for the Mo model $\tilde{\mathbf{1}}$.

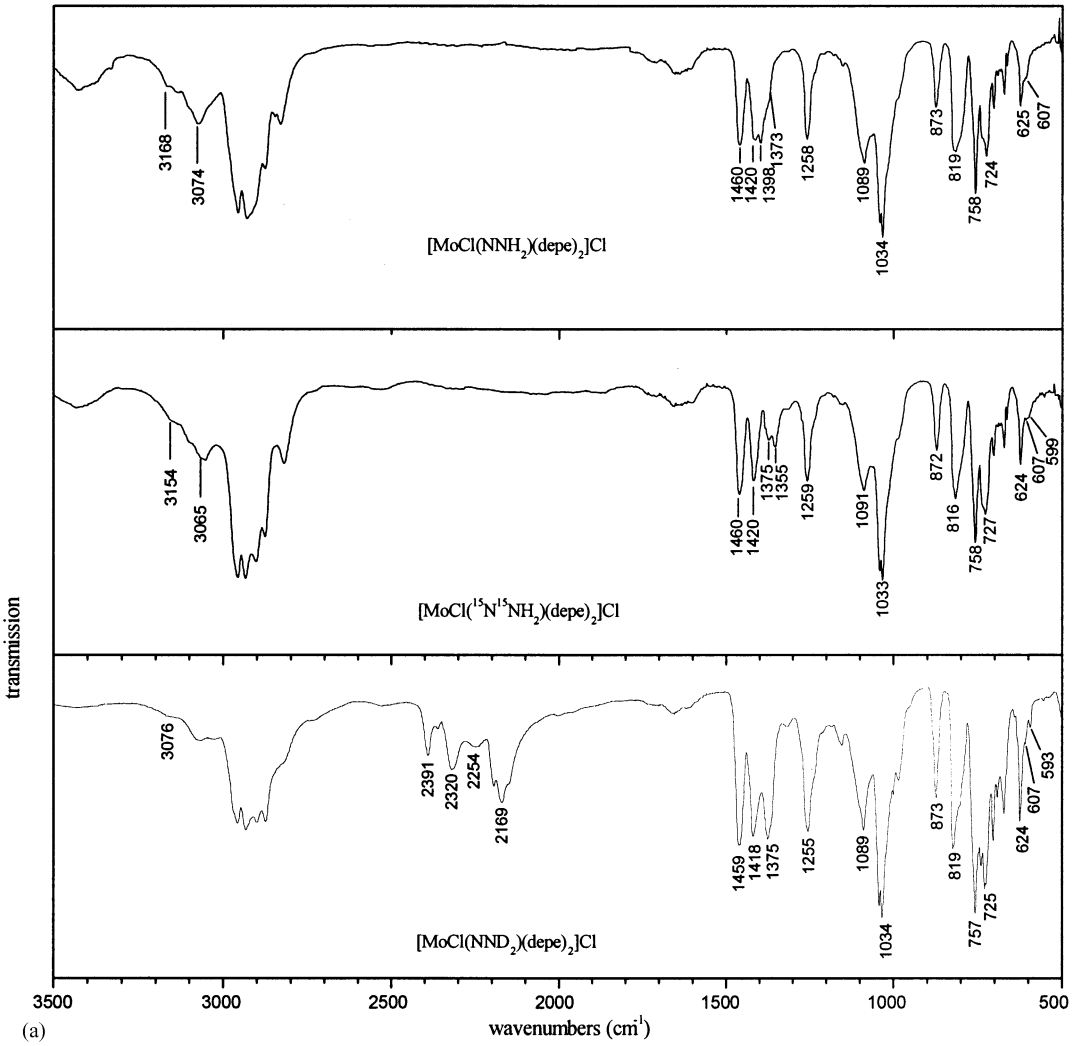

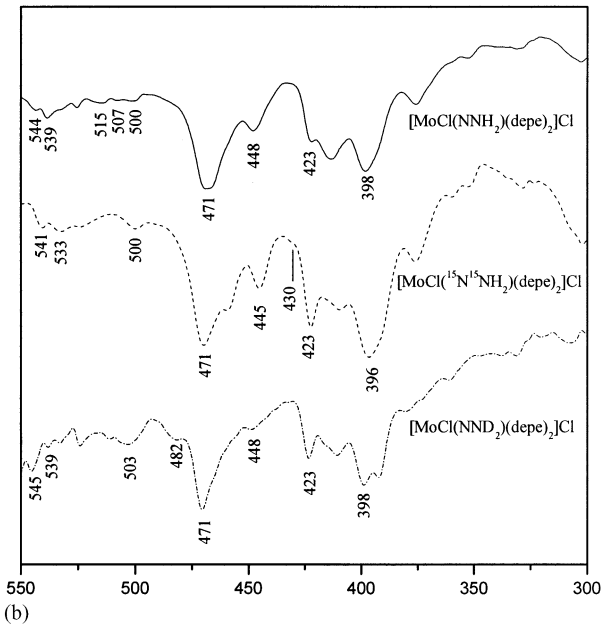

Fig. 6. MIR spectra of $[MoCl(NNH_2)(depe)_2]Cl$ (^{14}N-$\mathbf{3}^{Mo}_{depe}$), $[MoCl(^{15}N^{15}NH_2)(depe)_2]Cl$ (^{15}N-$\mathbf{3}^{Mo}_{depe}$) and $[MoCl(NND_2)(depe)_2]Cl$ (^{2}H-$\mathbf{3}^{Mo}_{depe}$) (b): FIR spectra of $[MoCl(NNH_2)(depe)_2]Cl$ (^{14}N-$\mathbf{3}^{Mo}_{depe}$), $[MoCl(^{15}N^{15}NH_2)(depe)_2]Cl$ (^{15}N-$\mathbf{3}^{Mo}_{depe}$) and $[MoCl(NND_2)(depe)_2]Cl$ (^{2}H-$\mathbf{3}^{Mo}_{depe}$).

Table 4
Force constants for $[M(N_2)_2(depe)_2]$, M = Mo ($\mathbf{1}^{Mo}_{depe}$) and W ($\mathbf{1}^{W}_{depe}$), and $[W(N_2)_2(dppe)_2]$

Force constant	Type	$[Mo(N_2)_2(depe)_2]$	$[W(N_2)_2(depe)_2]$	$[Mo(N_2)_2(dppe)_2]$ [a]	$[W(N_2)_2(dppe)_2]$
Y	M–N	2.37	2.54	2.04	2.66
Z	N–N	16.59	16.1	17.22	16.43
N_t	M–N: s/as	0.62	0.16	0.62	0.28
NN_t	N–N: s/as	0.35	0.39	0.35	0.28
N_s	M–N/N–N	1.25	1.25	1.25	0.96
N_st	M–N/N–N: s/as	−0.06	−0.05	−0.06	−0.13
Q	M–N–N	0.68	0.70	0.68	0.70
E	M–N–N: s/as	0.07	−0.09	0.07	0.10

$\mathbf{1}^{W}_{dppe}$; units are mdyn Å^{-1} for stretching and mdyn Å^{1} for bending interactions; the designations refer to Scheme 3.
[a] f(NN), f(MoN) and f(MoNN) adjusted from the force field of $[Mo(N_2)_2(depe)_2]$ to match the experimental frequencies of $[Mo(N_2)_2(dppe)_2]$ given in Table 7.

ν_s(MN) A_g	ν_s(NN) A_g	δ_s^x(MNN) B_{2g}	δ_s^y(MNN) B_{3g}	ν_{as}(MN) B_{1u}	ν_{as}(NN) B_{1u}	δ_{as}^x(MNN) B_{2u}	δ_{as}^y(MNN) B_{3u}
Y+N_t	N_s+N_st	0	0	0	0	0	0
N_s+N_st	Z+NN_t	0	0	0	0	0	0
0	0	Q-e	0	0	0	0	0
0	0	0	Q-e	0	0	0	0
0	0	0	0	Y-N_t	N_s-N_st	0	0
0	0	0	0	N_s-N_st	Z-NN_t	0	0
0	0	0	0	0	0	Q+e	0
0	0	0	0	0	0	0	Q+e

Scheme 3.

cluding the symbolic f matrix and the definition of the symmetry coordinates, have been described previously [7a].The symbolic F matrix of $\mathbf{1}'$ is shown in Scheme 3. Frequencies calculated by DFT (B3LYP) on model $\tilde{\mathbf{1}}$ and frequencies obtained with QCA-NCA on model $\mathbf{1}'$ are collected in Table 2 for $\mathbf{1}^{Mo}_{depe}$ and in Table 3 for $\mathbf{1}^{W}_{depe}$. Agreement between DFT frequencies and experimental values is satisfactory. The predicted N–N frequencies are within 2% of the observed values whereas the maximum deviation for the M–N frequencies is about 10%. The relatively poor reproduction of the experimental M–N frequencies is due to the simplification of the diphosphine ligands to PH_3 groups. Interestingly, the energetic sequence of ν_s(MN) and ν_{as}(MN) is different for the two systems: for $\mathbf{1}^{Mo}_{depe}$ (as for $\mathbf{1}^{W}_{dppe}$), ν_{as} is at higher frequency than ν_s whereas for $\mathbf{1}^{W}_{depe}$ the opposite is true. Table 4 presents the force constants of the central N–N–M–N–N unit of model $\mathbf{1}'$ resulting from QCA-NCA. Based on the force field of $[Mo(N_2)_2(depe)_2]$, the f(NN), f(MN) and f(MNN) force constants of $[Mo(N_2)_2(dppe)_2]$ were estimated by adjusting their values to fit the measured ^{14}N-frequencies of this system (there are no ^{15}N data available) [7a]. The N–N force constants of $\mathbf{1}^{Mo}_{depe}$ and $\mathbf{1}^{W}_{depe}$ are about equal, larger than for $\mathbf{1}^{W}_{depe}$ and smaller than for $\mathbf{1}^{Mo}{}_{dppe}$. This indicates a comparable activation of this ligand in the first two systems which is weaker than in $\mathbf{1}^{W}_{depe}$ and stronger than in $\mathbf{1}^{Mo}{}_{dppe}$. As a consequence, W is a stronger activating metal than Mo and depe is a stronger activating ligand than dppe. The metal–N force constants of $\mathbf{1}^{Mo}_{depe}$ and $\mathbf{1}^{Mo}{}_{dppe}$ are lower than in the two tungsten systems which is due to less diffuse *d* functions in Mo as compared to W.

4.2. *Mo–N_2H_2 complex* $\mathbf{3}^{Mo}_{depe}$

The infrared spectra of the isotopomeric 'hydrazido(2−)'-complexes ^{14}N-$\mathbf{3}^{Mo}_{depe}$, ^{15}N-$\mathbf{3}^{Mo}_{depe}$ and ^{2}H-$\mathbf{3}^{Mo}_{depe}$ are given in

Table 5
Observed and calculated frequencies of $[MoCl(NNH_2)(depe)_2]Cl$ ($\mathbf{3}^{Mo}_{depe}$) in cm^{-1}

	Experimental			QCA-NCA			B3LYP
	NNH_2	$^{15}N^{15}N_2$	NND_2	NNH_2	$^{15}N^{15}N_2$	NND_2	
ν_{as}(NH)$^{(1)}$	3168	3154	2391	3169	3159	2344	3707
ν_s(NH)$^{(1)}$	3076	3065	2254	3075	3069	2255	3557
ν_{as}(NH)$^{(2)}$	n.o.	n.o.	2320	3136	3127	2320	
ν_s(NH)$^{(2)}$	n.o.	n.o.	2169	2952	2945	2169	
ν(NN)	1398	1355	1374	1398	1353	1375	1451
ν_s(MoN)	544/539	541/533	545/539	569	556	549	627
ν_{as}(MoN)	607	599	593				
δ(MoNN)^{oop}	515	500	482	513	500	485	560
δ(MoNN)^{ip}		430		440	430	415	457

ν(MoCl)	ν(MoN)	ν(NN)	ν_s(NH)	δ_s(NNH)	τ	ν_{as}(NH)	δ_{as}(NNH)	δ^x(MoNN)	γ	δ^y(MoNN)
Y_1	N_t	N_sF	0	0	0	0	0	0	0	0
N_t	Y_2	N_s	$\sqrt{2}\,H^S_{MN}$	$\sqrt{2}\,H^B_{MN}$	0	0	0	0	0	0
N_sF	N_s	Z	$\sqrt{2}\,H^S_{NN}$	$\sqrt{2}\,H^B_{NN}$	0	0	0	0	0	0
0	$\sqrt{2}\,H^S_{MN}$	$\sqrt{2}\,H^S_{NN}$	H_s+H_st	H_{SB}+$H_{SB}t$	0	0	0	0	0	0
0	$\sqrt{2}\,H^B_{MN}$	$\sqrt{2}\,H^B_{NN}$	H_{SB}+$H_{SB}t$	H_B+H_Bt	0	0	0	0	0	0
0	0	0	0	0	T	0	0	0	0	0
0	0	0	0	0	0	H_s-H_st	H_{SB}-$H_{SB}t$	0	0	0
0	0	0	0	0	0	H_{SB}-$H_{SB}t$	H_B-H_Bt	0	0	0
0	0	0	0	0	0	0	0	Q_2	0	0
0	0	0	0	0	0	0	0	0	G	G_{lb}
0	0	0	0	0	0	0	0	0	G_{lb}	Q_1

Scheme 4.

Fig. 6a and b; Table 5 collects characteristic frequencies along with their isotope shifts and assignments. Interpretation of these spectra is based on the model system $[MoCl(NNH_2)P_4]^+$ (**3′**) of C_{2v} symmetry (Scheme 2). The central Cl–Mo–N–NH_2 unit of **3′** has 11 normal modes: the stretching vibrations ν_s(MoCl), ν(MoN), ν(NN) and ν_s(NH)/ν_{as}(NH), respectively, two N–N–H bending vibrations $\delta_{s/as}$(NNH), two linear bends $\delta^{ip/oop}$(MNN) ('in plane' (ip) and 'out of plane' (oop) refer to the NNH_2 plane), one out-of-plane γ bend at N_β and one torsion τ around the M–N–NH_2 axis. All of these vibrations are Raman active in C_{2v} and, with exception of the torsion, IR allowed. As Raman spectra of $\mathbf{3}^{Mo}_{depe}$ were found to be almost featureless, spectral analysis is based exclusively on IR data. This situation is analogous to that encountered for $\mathbf{3}^{W}_{dppe}$.

The region of the N–H stretching vibrations in the spectrum of ^{14}N-$\mathbf{3}^{Mo}_{depe}$ shows many bands of comparable intensity (Fig. 6a). In the spectrum of the deuterated compound ^{2}H-$\mathbf{3}^{Mo}_{depe}$, N–D vibrations are associated with two bands at 2391 and 2320 cm^{-1}, a weaker band at 2254 cm^{-1} and a more intense feature at 2169 cm^{-1}. In the case of $\mathbf{3}^{W}_{dppe}$, the appearance of two bands in the N–H stretching region was found to be compatible with the presence of two protons, giving rise to ν_s(NH) and ν_{as}(NH). Weaker, broadened features at lower energy were assigned to additional modes due to H-bridges between the complex cation and the anions [7a]. Based on the appearance of more than two N–D bands of comparable intensity in the spectrum of ^{2}H-$\mathbf{3}^{Mo}_{depe}$, hydrogen bonding between the NNH_2 unit and the Cl^- anions of $\mathbf{3}^{Mo}_{depe}$ must be much stronger than between the NNH_2 group and the BF_4^- counteranions of $\mathbf{3}^{W}_{dppe}$. Moreover, it is highly probable that the two chloride counterions of $\mathbf{3}^{Mo}_{depe}$ bridge two coordination units via hydrogen bonds. This would be analogous to $[WCl(NNH_3)(PMe_3)_4]Cl_2$ in which all hydrogen atoms of the NNH_3 group are H-bonded to Cl^- anions, two of these chloride ions forming a bridge between two complex molecules [12].

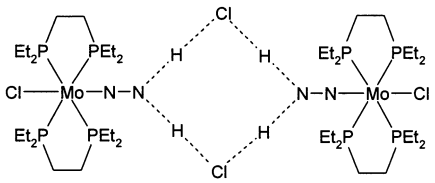

Fig. 7. Dimeric unit of $[MoCl(NNH_2)(depe)_2]Cl$.

Based on the hypothetical, chloride bridged structure of $\mathbf{3}^{Mo}_{depe}$ shown in Fig. 7, the N–H and N–D stretching features in Fig. 6a can be rationalized. The two vibrations ν_s(NH) and ν_{as}(NH) of the isolated NNH_2 unit double to two pairs $\nu_s^{(1)}/\nu_{as}^{(1)}$ and $\nu_s^{(2)}/\nu_{as}^{(2)}$, corresponding to symmetric and antisymmetric combinations of ν_s(NH) and ν_{as}(NH) in the dimer. In $\mathbf{3}^{W}_{dppe}$, the ν_s(NH)/ν_{as}(NH) splitting is found to be 77 cm^{-1}, increasing in the corresponding ^{2}H spectrum to 111 cm^{-1} [7a]. A comparable splitting is present in ^{14}N-$\mathbf{3}^{Mo}_{depe}$ if the features at 3168 and 3076 cm^{-1} are considered as one pair of s/as vibrations; e.g., $\nu_s^{(1)}/\nu_{as}^{(1)}$. As in $\mathbf{3}^{W}_{dppe}$, these features shift in the spectrum of ^{2}H-$\mathbf{3}^{Mo}_{depe}$, giving rise to the bands at 2391 and 2254 cm^{-1}. Consequently, the two remaining bands in the N–D stretching region of ^{2}H-$\mathbf{3}^{Mo}_{depe}$ at 2320 and 2169 cm^{-1} must correspond to the other s/as pair $\nu_s^{(2)}/\nu_{as}^{(2)}$. The ^{1}H counterpart of this second set of N–H vibrations in the 3000 cm^{-1} region is masked by intense vibrations of the depe ligand. The second isotope-sensitive feature in the MIR spectral region is a band at 1398 cm^{-1} which upon ^{15}N substitution shifts to 1355 cm^{-1} and upon deuteration to 1374 cm^{-1} and

Table 6
Force constants for $[MoCl(NNH_2)(depe)_2]Cl$ ($\mathbf{3}^{Mo}_{depe}$) and $[WF(NNH_2)(dppe)_2]BF_4$

Force constant	Type	$[MoCl(NNH_2)(depe)_2]Cl$	$[WF(NNH_2)(dppe)_2]BF_4$
Y_2	M–N	5.52	6.31
Z	N–N	7.16	7.19
$H_s^{(1)}$	N–H (1)	5.37	6.01
$H_s^{(2)}$	N–H (2)	5.10	–
$H_st^{(1)}$	N–H: s/as (1)	−0.07	−0.05
$H_st^{(2)}$	N–H: s/as (2)	−0.23	–
N_t	M–Cl/M–N	0.59	0.47
N_s	M–N/N–N	0.28	0.64
N_sf	M–Cl/N–N	0.32	0.32
Q_1	M–N–N	0.38	0.39
Q_2	M–N–N	0.67	0.70

$\mathbf{3}^{W}_{dppe}$; units are mdyn $Å^{-1}$ for stretching and mdyn $Å^1$ for bending interactions; the designations refer to Scheme 4.

Table 7
Characteristic frequencies of Mo/W–N_2, –NNH, –NNH_2 and –NNH_3 complexes in cm^{-1}

	Compound	ν(NN)	ν(MN)	ν(MNN)	Reference
$[W(N_2)_2(dppe)_2]$	$\mathbf{1}^{W}_{dppe}$	2007 (s)	419/414 (s)	555 (as)	[7a]
		1948 (as)	435 (as)		
$[Mo(N_2)_2(dppe)_2]$	$\mathbf{1}^{Mo}_{dppe}$	2033 (s)	393/404 (s)	550 (as)	[7a]
		1980 (as)	429(as) [a]		
$[W(N_2)_2(depe)_2]$	$\mathbf{1}^{W}_{depe}$	1968 (s)	434 (s)	557, 551 (as)	this work
		1907 (as)	403 (as)		
$[Mo(N_2)_2(depe)_2]$	$\mathbf{1}^{Mo}_{depe}$	1999 (s)	414 (s)	549 (as)	this work
		1932 (as)	426 (as)		
$[WF(NNH)(dppe)_2]$	$\mathbf{2}^{W}_{dppe}$	1457	530	514	[7a]
$[WF(NNH_2)(dppe)_2](BF_4)$	$\mathbf{3}^{W}_{dppe}$	1387	581	510/439	[7a]
$[MoCl(NNH_2)(depe)_2]Cl$	$\mathbf{3}^{Mo}_{depe}$	1398	607/544/539	515/440	this work
$[WF(NNH_3)(depe)_2](BF_4)_2$	$\mathbf{4}^{W}_{depe}$	1341 [b]	570	436	[8]
$[MoF(NNH_3)(depe)_2](BF_4)_2$	$\mathbf{4}^{Mo}_{depe}$	1386 [b]/1347 [c]	593 [b]/591 [c]	445 [b]/434 [c]	[8]

[a] B3LYP prediction; not observed.
[b] QCA-NCA prediction; not observed.
[c] Observed for ^{15}N labeled complex.

therefore is assigned to the N–N stretch. Interestingly, this band exhibits about the same ^{14}N-frequency as in the analogous compound $\mathbf{3}^{W}{}_{dppe}$ (1387 cm^{-1}), but a much larger intensity.

In agreement with the dimeric structure of $\mathbf{3}^{Mo}_{depe}$, the metal–N stretching vibration ν(MoN) and possibly the Mo–NN bending vibrations δ^{ip}(MNN) and δ^{oop}(MNN) are split into several components. Based on the DFT frequency calculation and experience from $\mathbf{3}^{W}_{dppe}$, both ν(MoN) and δ^{oop}(MoNN) of $\mathbf{3}^{Mo}{}_{depe}$ should be located above 471 cm^{-1}, the position of the depe band I, with ν(MN) being at higher energy than δ^{oop}(MNN) (Table 5). Bands at 544 and 539 cm^{-1} in the spectrum of ^{14}N-$\mathbf{3}^{Mo}_{depe}$ which shift to 541 and 533 cm^{-1} in the spectrum of ^{15}N-$\mathbf{3}^{Mo}_{depe}$, respectively, are assigned to vibrations of ν(MN) character (Fig. 6b). Remarkably, these vibrations do not shift in the spectrum of ^{2}H-$\mathbf{3}^{Mo}_{depe}$. An additional isotope-sensitive band is found at 607 cm^{-1} (^{14}N), shifting to 599 and 593 cm^{-1} in the spectra of the ^{15}N- and ^{2}H-substituted compound, respectively (Fig. 6a). Based on the dimeric structure of $\mathbf{3}^{Mo}_{depe}$, we assign this vibration to the antisymmetric combination of W–N stretches whereas the bands at 544 and 539 cm^{-1} are assigned to the symmetric combination of the W–N stretches. The lack of ^{2}H isotope shift of the latter features is attributed to the fact that the symmetric combination of W–N stretches entails little motion of the H(D) atoms involved in the hydrogen bonds to the bridging chloride ions, basically corresponding to a vibration of the two N–N units towards each other. In contrast, there is significant motion of the H(D) atoms involved in the antisymmetric combination of W–N stretches, being in agreement with the considerable ^{2}H isotope shift of this vibration.

Spectral comparison between the ^{14}N and the ^{15}N spectrum of $\mathbf{3}^{Mo}{}_{depe}$ further suggests that the band at 515 cm^{-1} in the spectrum of ^{14}N-$\mathbf{3}^{Mo}{}_{depe}$ which shifts to 500 cm^{-1} in the spectrum of ^{15}N-$\mathbf{3}^{Mo}{}_{depe}$ is associated with δ^{oop}(MNN). In the latter spectrum it is superimposed with another band at 500 cm^{-1} which does not appear to shift. In the spectrum of ^{2}H-$\mathbf{3}^{Mo}{}_{depe}$, the δ^{oop} vibration shifts to 482 cm^{-1}. Based on the calculation and comparison with $\mathbf{3}^{W}_{dppe}$, the in-plane MoNN bending vibration δ^{ip} should be around 430 cm^{-1}, exhibiting a ^{15}N shift of -10 cm^{-1}. The ^{15}N-spectrum exhibits a shoulder at 430 cm^{-1} which could be associated with this vibration.

DFT frequency calculations on $\mathbf{3}^{Mo}{}_{depe}$ are based on model $\tilde{\mathbf{3}}$ (Fig. 1) and have been performed as described in Ref. [7b]. Modification of $\tilde{\mathbf{3}}$ gives model $\mathbf{3}'$ (Scheme 2) which is used for QCA-NCA. The symbolic F matrix for model system $\mathbf{3}'$ is shown in Scheme 4. Calculated (B3LYP) frequencies and frequencies obtained with the QCA-NCA procedure are collected in Table 5 along with the measured data. Agreement between the frequencies calculated by DFT and the experimentally determined values is less good than for $\mathbf{3}^{W}_{dppe}$. This is due to the dimeric structure of $\mathbf{3}^{Mo}_{depe}$ which is not taken into account in the DFT calculation. In the QCA-NCA procedure, these discrepancies are partly removed, giving overall good agreement with the measured data. Isotope shifts are reproduced quite well, with exception of the 2391 cm^{-1} N–D band which is calculated at 2344 cm^{-1}. The Mo–N force constant is determined to reproduce the averages of the observed Mo–N stretching frequencies in the dimer. Table 6 collects the force constants of the central Cl–M–N–N unit of model $\mathbf{3}'$ resulting from QCA-NCA. The values are generally similar to those found for $\mathbf{3}^{W}_{dppe}$, with exception of the metal–N force constant Y_2 which for $\mathbf{3}^{Mo}_{depe}$ is lower (5.52 mdyn $Å^{-1}$) than found for $\mathbf{3}^{W}_{dppe}$ (6.31 mdyn $Å^{-1}$). Due to the presence of bridging Cl^- ions, the N–H stretching force constant H_s of $\mathbf{3}^{Mo}_{depe}$ (5.37 mdyn $Å^{-1}$) is also lower than that found for $\mathbf{3}^{W}_{dppe}$ (6.01 mdyn $Å^{-1}$).

Table 8
Force constants of Mo/W–N_2, –NNH, –NNH_2 and –NNH_3 complexes (units are mdyn Å^{-1} for stretching and mdyn Å^1 for bending modes)

	Compound	f(NN)	f(MN)	f(MNN)	Reference
$[W(N_2)_2(dppe)_2]$	$\mathbf{1}^{W}_{dppe}$	16.43	2.66	0.70	[7a]
$[W(N_2)_2(depe)_2]$	$\mathbf{1}^{W}_{depe}$	16.1	2.54	0.70	this work
$[Mo(N_2)_2(depe)_2]$	$\mathbf{1}^{Mo}_{depe}$	16.59	2.37	0.68	this work
$[Mo(N_2)_2(dppe)_2]$	$\mathbf{1}^{Mo}_{dppe}$	17.22	2.04	0.68	this work [a]
$[WF(NNH)(dppe)_2]$	$\mathbf{2}^{W}_{dppe}$	8.27	4.50	0.53	[7a]
$[WF(NNH_2)(dppe)_2](BF_4)$	$\mathbf{3}^{W}_{dppe}$	7.20	6.31	0.39/0.69	[7a]
$[MoCl(NNH_2)(depe)_2]Cl$	$\mathbf{3}^{Mo}_{depe}$	7.16	5.52	0.38/0.67	this work
$[WF(NNH_3)(depe)_2](BF_4)_2$	$\mathbf{4}^{W}_{depe}$	6.03	7.31	0.65	[8]
$[MoF(NNH_3)(depe)_2](BF_4)_2$	$\mathbf{4}^{Mo}_{depe}$	6.03	8.01	0.63	[8]

[a] See Table 4.

5. Discussion

In the preceding sections the vibrational structures of Mo and W–N_2 and –N_2H_2 complexes with depe coligands have been derived. This subject is of interest with respect to the generation of NH_3 from dinitrogen, mediated by Mo and W phosphine systems. The protonation of complex-bound N_2 requires an 'activation' of this ligand which corresponds to the transfer of electronic charge from the metal into the π* orbitals of dinitrogen. As this acts to increase the N–N bondlength and lower the N–N stretching frequency, the reduction of ν(NN) from its free-molecule value (2330 cm^{-1}) has been taken as a measure of activation [21].

We have extended this methodology into several directions. First of all, we have carried out detailed vibrational-spectroscopic studies on Mo– and W–N_2 complexes, allowing to also determine the frequencies of metal–ligand vibrations. These vibrational-spectroscopic studies were complemented by DFT calculations, providing theoretical estimates of vibrational frequencies and force constants as well as electronic-structure information on the investigated compounds. Based on this information, QCA-NCA's were performed on these systems, giving metal–N and N–N force constants (Table 8) [7,19,22]. Using this approach, we also studied the protonated derivatives of dinitrogen complexes, i.e. M–NNH, M–NNH_2 and M–NNH_3 compounds with M = Mo and W [7,8,22]. While our previous investigations were mainly carried out on Mo and W dppe systems, the present paper gives complementary information for Mo and W depe complexes.

Consideration of the N–N and metal–N force constants of the N_2 complexes and their protonated intermediates provides insight into the ligand activating properties of the various metal–$(diphos)_2$ combinations and allows to monitor the state of the N_2H_x ligand upon successive protonation (Table 8, Fig. 8). Trends obtained from the f(NN) values of the N_2 complexes are in line with those derived from the N–N frequencies; i.e. $[W(N_2)_2(dppe)_2]$ and $[Mo(N_2)_2(depe)_2]$ provide the same activation of N_2 which is weaker than in case of $[W(N_2)_2(depe)_2]$ and stronger than in the case of $[Mo(N_2)_2(dppe)_2]$. Therefore, tungsten is a stronger activating metal than molybdenum and depe is a stronger activating coligand than dppe [21] At the stage of the N_2 complex, the weaker activation by dppe can be compensated by a stronger activating metal, explaining the comparable N_2 activation found in $[Mo(N_2)_2(depe)_2]$ and $[W(N_2)_2(dppe)_2]$. As can be inferred from the metal–N force constants (Table 8), W in general exhibits a stronger metal–N_2 bond than Mo, corresponding to a larger back-bonding interaction and therefore a stronger activation of N_2. This is due to more diffuse *d* functions for W than for Mo. The stronger activation of N_2 by depe as compared to dppe, on the other hand, is caused by a stronger σ-donor and/or weaker π-acceptor capability of the former as compared to the latter ligand. This is obviously the primary factor responsible for the formation of hydrazidium complexes, accounting for the fact that both $[Mo(N_2)_2(depe)_2]$ and $[W(N_2)_2(depe)_2]$ can be protonated with HBF_4 to hydrazidium complexes whereas this is not possible with their Mo and W dppe analogs [10].

Protonation of the depe complexes $[Mo(N_2)_2(depe)_2]$ and $[W(N_2)_2(depe)_2]$ with HCl, on the other hand, leads

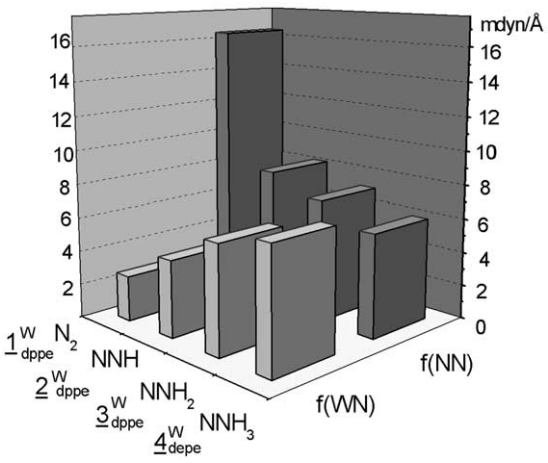

Fig. 8. Evolution of M–N and N–N force constants.

to NNH_2 compounds [8]. For the $[MoCl(NNH_2)(depe)_2]Cl$ complex generated this way, the N–N force constant (7.16 mdyn $Å^{-1}$) is similar to the value of $[WF(NNH_2)(dppe)_2](BF_4)$ (7.19 mdyn $Å^{-1}$). However, the metal–N force constant of $[MoCl(NNH_2)(depe)_2]Cl$ (5.52 mdyn $Å^{-1}$) is lower than found for the W–NNH_2 dppe complex (6.31 mdyn $Å^{-1}$, cf. Table 6). We ascribe this discrepancy to a dimeric structure of the Mo–depe complex (in contrast to the W–dppe complex which is monomeric), leading to a splitting of the Mo–N stretches into a symmetric and an antisymmetric combination. The metal–N force constant of 5.52 mdyn $Å^{-1}$ reproduces the *average* frequency of these split vibrations and therefore is not strictly comparable to the W–N force constant of the monomeric complex $[WF(NNH_2)(dppe)_2](BF_4)$. In the proposed dimeric structure of $[MoCl(NNH_2)(depe)_2]Cl$, two complex molecules are bridged by two Cl^- anions. This is analogous to the structure of $[WCl(NNH_3)(PMe_3)_4]Cl_2$ with the only difference that in the latter compound each hydrazido group is bound to one additional proton which in turn is hydrogen-bonded to a terminal Cl^- anion [12]. Hydrogen bridges also exist in NNH_x complexes with BF_4 counterions (vide supra), but obviously they are much weaker than in the corresponding compounds containing chloride anions.

Upon protonation of $[W(N_2)_2(dppe)_2]$ to the NNH complex $[WF(NNH)(dppe)_2]$, the N–N force constant decreases from about 16 mdyn $Å^{-1}$ to a value of 8.27 mdyn $Å^{-1}$ and the M–N force constant increases from a value of about 2.5 to 4.5 mdyn $Å^{-1}$ (Fig. 8, Table 8) [7a]. This trend continues in the next protonation steps; i.e. for $[WF(NNH_2)(dppe)_2]^+$ the N–N force constant is further reduced to a value of 7.2 mdyn $Å^{-1}$ and the metal–N force constant further increases to 6.3 mdyn $Å^{-1}$. In the NNH_3 complexes $[MF(NNH_3)(depe)_2]^{2+}$, M = Mo or W, the N–N force constant is found to be 6.03 mdyn $Å^{-1}$, close to the value of an N–N single bond, while the metal–N force constants (8.01 and 7.31 mdyn $Å^{-1}$, respectively) reach values typical for a metal–N triple bond [8]. In contrast to the N–N and metal–N force constants, the MNN bending force constants remain approximately constant upon successive protonation (around 0.7 mdyn $Å^{-1}$), with exception of the in-plane bending force constants in the NNH_2 systems which exhibit values of about 0.4 mdyn $Å^{-1}$.

The experimentally determined evolution of N–N force constants upon stepwise protonation indicates a successive decrease in N–N bond order, thus initiating bond cleavage, whereas the evolution of metal–N force constants reflects an increase of metal–ligand covalency, indicative of a successive strengthening of the metal–N bond. Besides providing an energetic driving force for the reduction of the N–N triple bond, this also acts to prevent loss of partly reduced NNH_x substrate, $x = 1$–3, in the course of the transformation of N_2 to ammonia. The next step in this process is the cleavage of the N–N bond, leading to nitrido or imido systems. This requires addition of electrons from an external source as octahedral NNH_3 systems with diphosphine ligation are inert to N–N cleavage [8]. Spectroscopic investigations of both the cleavage of the N–N bond and the post-NN cleavage phase of N_2 reduction and protonation are underway [23].

Acknowledgements

Funding of this research by the State of Schleswig-Holstein and financial support by DFG (Tu58-04 and 05) and FCI are gratefully acknowledged.

References

[1] M.D. Fryzuk, S.A. Johnson, Coord. Chem. Rev. 200 (2000) 379.
[2] E.W. Triplett (Ed.), Prokaryotic Nitrogen Fixation: A Model System for the Analysis of a Biological Process, Horizon Scientific Press, 2000.
[3] O. Einsele, A.F. Tezcan, S.L.A. Andrade, B. Schmid, M. Yoshida, J.B. Howard, D.C. Rees, Science 297 (2002) 1696.
[4] F. Tuczek, N. Lehnert, Angew. Chem. Int. Ed. 37 (1998) 2636.
[5] (a) G.J. Leigh, Accounts Chem. Res. 25 (1992) 177;
(b) R.A. Henderson, G.J. Leigh, C. Pickett, Adv. Inorg. Chem. Radiochem. 27 (1983) 197;
(c) M. Hidai, Y. Mizobe, Chem. Rev. 95 (1995) 1115.
[6] R.N.F. Thorneley, D.J. Lowe, in: T.G. Spiro (Ed.), Molybdenum Enzymes, John Wiley, New York, 1985.
[7] (a) N. Lehnert, F. Tuczek, Inorg. Chem. 38 (1999) 1659;
(b) N. Lehnert, F. Tuczek, Inorg. Chem. 38 (1999) 1671.
[8] K.H. Horn, N. Lehnert, F. Tuczek, Inorg. Chem. 42 (2003) 1076.
[9] (a) M. Jimenez-Tenorio, M.C. Puerta, P. Valerga, D.L. Hughes, J. Chem. Soc. Dalton Trans. (1994) 2431;
(b) T.A. George, B.B. Kaul, Q. Chen, Zubieta, J. Inorg. Chem. 32 (1993) 1706;
(c) T.A. George, L. Ma, S.N. Shailh, S.N. Tisdale, R.C., J. Zubieta, Inorg. Chem. 29 (1990) 4789;
(d) A. Galindo, A. Hills, D.L. Hughes, R.L. Richards, M. Hughes, J. Mason, J. Chem. Soc. Dalton Trans. (1990) 283;
(e) J.E. Barclay, A. Hills, D.L. Hughes, G.J. Leigh, C.J. Macdonald, M. Abu Bakar, H. Mohd.-Ali, J. Chem. Soc. Dalton Trans. (1990) 2503;
(f) M. Abu Bakar, D.L. Hughes, W. Hussain, G.J. Leigh, C.J. Macdonald, H. Mohd.-Ali, J. Chem. Soc. Dalton Trans. (1988) 2545;
(g) T.A. George, R.C. Tisdale, J. Am. Chem. Soc. 107 (1985) 5157;
(h) J. Chatt, M.E. Fakley, P.B. Hitchcock, R.L. Richards, N.T. Luong-Thi, J. Chem. Soc. Dalton Trans. (1982) 345;
(i) T. Takahasi, Y. Mizobe, M. Sato, Y. Uchida, M. Hidai, J. Am. Chem. Soc. 102 (1980) 7461;
(j) J. Chatt, A.J. Pearman, R.L. Richards, J. Chem. Soc. Dalton Trans. (1978) 1766;
(k) J. Chatt, A.J. Pearman, R.L. Richards, J. Chem. Soc. Dalton Trans. (1977) 2139;
(l) J. Chatt, A.J. Pearman, R.L. Richards, J. Chem. Soc. Dalton Trans. (1977) 1852;
(m) J. Chatt, A.J. Pearman, R.L. Richards, J. Chem. Soc. Dalton Trans. (1976) 1520;
(n) G.A. Heath, R. Mason, K.M. Thomas, J. Am. Chem. Soc. 96 (1974) 260;
(o) J. Chatt, G.A. Heath, R.L. Richards, J. Chem. Soc. Dalton Trans. (1974) 2074;
(p)J. Chatt, G.A. Heath, R.L. Richards, J. Chem. Soc. Chem. Commun. (1972) 1010.
[10] J.E. Barclay, A. Hills, D.L. Hughes, G.J. Leigh, C.J. Macdonald, M. Bakar, H. Ali, J. Chem. Soc. Dalton Trans. (1990) 2503.

[11] W. Hussain, G.J. Leigh, H. Mohd. Ali, C.J. Pickett, D.A. Rankin, J. Chem. Soc. Dalton Trans. (1984) 1703.
[12] (a) A. Galindo, A. Hills, D.L. Hughes, R.L. Richards, J. Chem. Soc. Chem. Commun. (1990) 283;
(b) A. Galindo, A. Hills, D.L. Hughes, R.L. Richards, J. Chem. Soc. Chem. Commun. (1987) 1815.
[13] A.D. Becke, J. Chem. Phys. 98 (1993) 5648.
[14] T.H. Dunning, P.J. Hay, in: H.F. Schaefer (Ed.), Modern Theoretical Chemistry, Plenum, New York, 1976.
[15] (a) P.J. Hay, W.R. Wadt, J. Chem. Phys., 82 (1985), 270 and 299.;
(b) W.R. Wadt, P.J. Hay, J. Chem. Phys. 82 (1985) 284.
[16] A. Allouche, J. Pourcin, Spectrochim. Acta 49A (1993) 571.
[17] T. Miyazawa, J. Chem. Phys. 29 (1958) 246.
[18] J.A. Nelder, R. Mead, Comput. J. 7 (1965) 308.
[19] O. Franke, B.E. Wiesler, N. Lehnert, F. Tuczek, Z. Anorg. Allg. Chem. 628 (2002) 2395.
[20] (a) U. Posset, W. Kiefer, Vib. Spectrosc. 3 (1992) 47;
(b) U. Posset, W. Kiefer, J. Mol. Struct. 349 (1995) 427.
[21] (a) J. Chatt, J.R. Dilworth, R.L. Richards, Chem. Rev. 78 (1978) 589;
(b) W. Hussain, G.J. Leigh, H. Mohd. Ali, C.J. Pickett, D.J. Rankin, J. Chem. Soc. Dalton Trans. (1984) 1703.
[22] C.M. Habeck, N. Lehnert, C. Näther, F. Tuczek, Inorg. Chim. Acta 337C (2002) 11, and references cited therein.
[23] N. Böres, K. Mersmann, K.H. Horn, N. Lehnert, F. Tuczek, manuscript in preparation.